ARTICLE

# Unveiling the Efficiency of Microwave-Assisted Hydrothermal Treatment for the Preparation of $SrTiO_3$ Mesocrystals

Received 00th January 20xx,
Accepted 00th January 20xx

DOI: 10.1039/x0xx00000x

Luís F. da Silva,*[a] Ariadne C. Catto,[a] Waldir Avansi Jr,[a] Alexandre Mesquita,[b] Lauro J. Q. Maia,[c] Osmando F. Lopes,[d] Máximo Siu Li,[e] Mário L. Moreira,[f] Elson Longo,[g] Juan Andrés[h] and Valmor R. Mastelaro[e]

*Materials processing has become essential for the proper control, tuning and consequent application of the properties of micro/nanoparticles. In this case, we report herein the capability of the microwave-assisted hydrothermal (MAH) method to prepare $SrTiO_3$ compound, as a case study of inorganic compounds. Analyses conducted by X-ray diffraction, X-ray photoelectron and X-ray absorption spectroscopies confirmed that the MAH route enables the formation of pristine $SrTiO_3$. The results indicated that the combination of thermal and non-thermal effects during the MAH treatment provides ideal conditions for an efficient and rapid synthesis of pristine $SrTiO_3$ mesocrystals. Scanning electron microscopy images revealed a cube-like morphology (of ca. 1 µm) formed via a self-assembly process, influenced by the MAH time. Additionally, photoluminescence measurements revealed a broad blue emission related to intrinsic defects, which decreased with MAH synthesis time.*

## 1. Introduction

The processing of ceramic materials with multifunctional properties has been attracting the attention of researchers[1–9] aiming to prepare micro/nanostructured inorganic semiconductors through the exploration of a variety of physical and chemical approaches.[2,10–17] Despite their capability in obtaining such semiconductors, most of approaches spend a large amount of energy and require long synthesis times.[2,13,14,18–20] In this context, the microwave-assisted hydrothermal (MAH) route has been considered a clean, versatile, fast, and highly efficient method to obtain organic and inorganic compounds.[7,21–23] The microwave energy has the potential to be ubiquitous and greatly contribute to the synthesis of materials in almost all areas of synthetic chemistry fields,[2,7,13,14,18,19,24,25] considering that it requires short times and relatively low temperatures (usually < 200 °C) in comparison with conventional heating methods.[14,26] This route also contributes to suppress side reactions, improving the reproducibility degree.[10,13,14]

In the 1990, Komarneni and co-workers investigated the preparation of oxide materials via microwave-assisted treatment.[2] They reported that this methodology improved the crystallization kinetics of various inorganic compounds.[2] In the past years, there has been an increasing interest in improving the MAH route for the synthesis of micro/nanocrystals, since it provides not only a simple and fast way to obtain these materials but also because its homogeneous heating minimizes thermal gradient effects with the formation of oriented structures with unique or enhanced properties.[13,14,18,19,27]

De La Hoz and co-workers described that the importance of microwave irradiation during chemical synthesis could be related to thermal and non-thermal effects.[19] According to the authors, the thermal effects are the solution superheating and the presence of hot-spots, while the non-thermal effects are the highly polarized electric field and those related to mobility and diffusion that increase the probabilities of effective contacts.[19]

Motivated by such versatility and efficiency, the MAH method has been used to obtain different micro/nanocrystalline compounds.[13,14,19,28–30] Strontium titanate ($SrTiO_3$) has attracted attention because of its remarkable multifunctional properties.[3,31–37] Moniruddin and co-workers demonstrated the potential of pristine $SrTiO_3$ nanoparticles as catalysts for the production of $H_2$ gas via water-splitting process.[35] In the past decade, our research group studied the pristine and doped nanostructured $SrTiO_3$ applied as photocatalysts and gas-sensing layer. To do so, different methodologies were used, such as electron beam vapor deposition, polymeric precursor method, conventional hydrothermal and MAH method.[24,38–43] Regarding the MAH route, it was successfully used to prepare of $SrTiO_3$ powders, allowing a proper control over the crystal

[a] Laboratory of Nanostructured Multifunctional Materials, Federal University of São Carlos, Rodovia Washington Luiz, km 235, 13565-905, São Carlos, SP, Brazil. E-mail: lfsilva83@gmail.com; TEL +55 16 35091524.
[b] Department of Physics, IGCE, São Paulo State University, P.O. Box 178, 13500-970, Rio Claro, SP, Brazil.
[c] Institute of Physics, Federal University of Goiás, Alameda Palmeiras s/n, 74690-900, Goiânia, GO, Brazil.
[d] Institute of Chemistry, Federal University of Uberlândia, 38400-902, Uberândia, MG, Brazil.
[e] Institute of Physics of São Carlos, University of São Paulo, Avenida Trabalhador São Carlos, 13566-590, São Carlos, SP, Brazil.
[f] INCTMN, Physical and Mathematics Institute (IFM), Universidade Federal de Pelotas, Campus Universitário Capão do Leão, 96010-900, Pelotas, RS, Brazil
[g] Center for Development of Functional Materials, Federal University of São Carlos, Rodovia Washington Luiz, km 235, 13565-905, São Carlos, SP, Brazil.
[h] Departamento Química-Física y Analítica, Universitat Jaume I, Castelló E-12080, Spain.

† Electronic Supplementary Information (ESI) available: XRD patterns and FTIR spectra of samples SAM2, SAM3 and SAM4. See DOI: 10.1039/x0xx00000x

shape, photoluminescence properties and assembly process of the nanoparticles by an appropriate choice of titanium precursor as well as synthesis time.[23,24,27,39]

In one of these previous studies, we demonstrated the relationship between structural properties and photocatalytic activity of $SrTiO_3$ obtained via MAH route, where we could observe a high disorder degree in the local structure around Ti atoms beyond the presence of some fivefold coordinated Ti atoms, leading to a photocatalytic improvement of the as-obtained samples of pristine $SrTiO_3$.[24] Following this line of research, this work aimed of this work is threefold: (i) to demonstrate the efficiency and potentiality of the MAH method in obtaining of pristine $SrTiO_3$ crystals; (ii) to show the potential of this route for designing functional materials with superior properties and; (iii) to present and investigate the relationship between microwave-assisted hydrothermal treatment and photoluminescent properties. To achieve these purposes, different techniques such as X-ray diffraction (XRD), X-ray absorption near edge structure (XANES) spectroscopy, X-ray photoelectron spectroscopy (XPS), electron paramagnetic resonance (EPR), photoluminescence (PL) spectroscopy, and field emission scanning electron microscopy (FE-SEM) were employed to characterize the obtained samples.

## 2. Experimental Section

### 2.1. Synthesis and characterization of $SrTiO_3$

To evaluate the effect of the MAH treatment on the preparation of the $SrTiO_3$ compound, two reaction mixtures were prepared, as reported in Ref 24. Strontium chloride ($SrCl_2.6H_2O$; 99.9 %) and titanium oxysulfate ($TiOSO_4.xH_2SO_4.yH_2O$ solution; 99.9 %) reagents purchased from Sigma-Aldrich Corporation were used. First, $TiOSO_4$ and $SrCl_2$ (0.01 M, Sr: Ti = 1: 1) were added to 50 mL of deionized water, followed by another 50 mL of 6 M KOH solution under constant stirring for 30 min. Afterwards, the reaction mixture was washed with deionized water and isopropyl alcohol, and then dried for 12 h at 80 °C. The obtained sample was labelled as SAM1.

#### 2.1.1. MAH synthesis *vs*. thermal annealing

In order to demonstrate the efficiency of the MAH synthesis compared to conventional thermal annealing, the sample SAM1 was weighted and then divided into three equal portions. Two portions were annealed in an electric oven under air atmosphere for 2 h, one at 300 °C, and the other at 750 °C, both at a heating rate of 10 °C $min^{-1}$. The last portion of the sample was maintained as-obtained, i.e., without any treatment.

#### 2.1.2. Longer MAH synthesis time

To study the influence of synthesis time, the precursor solution was heat-treated in the MAH system for 10 min (SAM2), 320 min (SAM3), and 640 min (SAM4). To this end, the reaction mixture was put into a 110 mL Teflon autoclave, which was in turn sealed and placed inside the custom-built microwave-assisted hydrothermal (MAH) system. The solution was then treated at 140 °C with a heating rate of 140 °C $min^{-1}$ under an auto-generated pressure of 3 bar. At the end of the synthesis, the precipitated powder was washed and dried following the same procedure steps abovementioned.

### 2.2. Characterization techniques

The samples were characterized by X-ray diffraction (XRD) in a 2θ= 20 to 60° with a step size of 0.02°, at a scanning speed of 2°$min^{-1}$, using CuKα radiation (Rigaku, RotaflexRU200B). The structure was refined using the Rietveld method and the General Structure Analysis System (GSAS) package with the EXPGUI graphical user interface. The average crystallize size was estimated from the FWHM of (110) XRD peak in the Scherrer's equation.[38] The FWHM value of the XRD peak due to instrumental broadening was considered using Si sample a as reference. X-ray absorption near-edge structure (XANES) measurements were performed at the XAFS2 beamline at the Brazilian Synchrotron Light Laboratory (LNLS). The Ti K-edge XANES spectra were collected in transmission mode at room temperature in the range of 4910 to 5200 eV with an energy step size of 0.3 eV around the edge, following the already reported experimental conditions.[31,36,44] For the XANES analysis, the background was removed from all the spectra, which were then normalized by the first extended X-ray absorption fine structure (EXAFS) oscillation using MAX software.[45] X-ray photoelectron spectroscopy (XPS) analyses were performed on a ScientaOmicron (model ESCA+) spectrometer using monochromatic AlKα (hv= 1486.6 eV) radiation. The binding energies were corrected for charging effects by assigning a value of 284.8 eV to the adventitious C 1s line.

Morphological properties of the samples were characterized using a field emission scanning electron microscope (FE-SEM, Zeiss Supra35) operated at 5 kV in different magnifications. Room-temperature photoluminescence (PL) spectra were collected using a Thermal Jarrel-Ash Monospec 27 monochromator and a Hamamatsu R446 photomultiplier linked with a data acquisition system consisting of an SR-530 lock. All samples were excited by 350 nm wavelength light from a krypton ion laser (Coherent Innova) and the nominal output power of the laser was kept at 200 mW.

EPR measurements were performed at 10 K using 10 mg of the sample, introduced into a quartz EPR tubes together of a secondary standard *g* marker of MgO:Cr(III) with EPR *g* = 1.9797 signal calibrated with weak pitch standard. A Varian X- band spectrometer (model E-109) operating at a center Field of 3300 G, sweep field of 500 G, sweep time of 120 s, and MW frequency of 9.136 GHz.

## 3. Results and Discussion

### 3.1. The efficiency of MAH approach

XRD patterns of the samples SAM1 (before MAH treatment) and SAM2 (after MAH treatment) samples are shown in Fig. 1. The XRD pattern of SAM1 can be indexed to various crystalline phases identified as: $SrTiO_3$ (JCPDS file 35-0734), $SrSO_4$ (JCPDS file 05-0593), $SrCl_2.6H_2O$ (JCPDS file 06-0073), $SrCO_3$ (JCPDS file 05-0418) and $K_2Ti_6O_{13}$ phase (JCPDS file 74-0275). In contrast, XRD pattern of SAM2 reveals that when submitted to MAH treatment, it exhibits only reflections assigned to cubic perovskite $SrTiO_3$ phase.[23,24,27]

Before MAH treatment, the reactants were mixed under alkaline conditions at room temperature to form the aforementioned crystalline phases, being the $SrSO_4$ the major phase found. This may be associate with the low solubility of $SrSO_4$ under alkaline ($K_{sp}$ = 3.8 x $10^{-7}$) conditions.[46] Nevertheless, when the reactional mixture undergoes MAH treatment, the pristine $SrTiO_3$ phase can be obtained, as seen in Fig. 1. Some researchers described that the hydrothermal route, especially the microwave-assisted one, enhances the solubility and mobility of the ionic species as a result of

water viscosity and polarization reductions related to the electric field component of the electromagnetic wave.[14,46] Therefore, such treatment is capable of solubilizing $SrSO_4$, thus providing Sr(II) ions to react with Ti species, consequently forming pristine $SrTiO_3$.

**Fig.1** XRD patterns of samples SAM1 and SAM2.

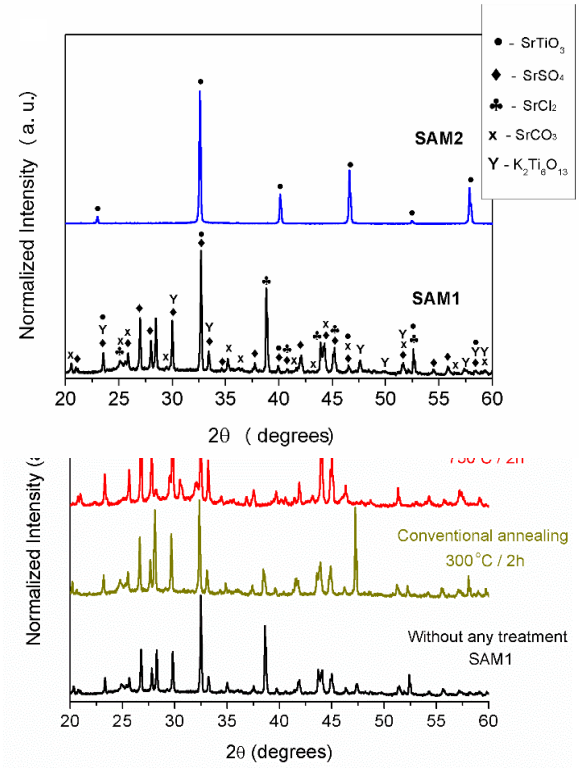


To confirm the efficiency of the MAH method to obtain the $SrTiO_3$ pristine compound, the as-obtained sample SAM1 was annealed in an electric oven for 2 h at 300 °C, and 750 °C. The XRD patterns of the samples after thermal annealing are shown in Fig. 2. All samples presented a mixture of crystalline phases. It is interesting to note that independently of the annealing temperature (in the range here investigated), the conventional heating was ineffective in providing the necessary conditions to obtain the pristine $SrTiO_3$. Therefore, the presented results confirm the efficiency of the MAH method in synthetizing a pure $SrTiO_3$ compound in a shorter time and at a lower temperature.

**Fig.2** XRD patterns of the sample SAM1 as-obtained (without any treatment), and then annealed in an electric oven for 2 hours at 300°C, and 750°C.

### 3.2. The influence of longer MAH synthesis time

To obtain further details on the processing of $SrTiO_3$ compound through the MAH method, we studied the influence of longer MAH synthesis time on the local structure around Ti atoms, on the surface electronic structure, and on the PL emission of the compound. For this purpose, the reactional mixtures were treated in the MAH system at 140°C for 10 min (SAM2), 320 min (SAM3) and 640 min (SAM4), where the synthesis parameters, such as pressure, heating rate and precursors and their concentrations, were kept constant. Fig.S1 and Fig.S2 (ESI†) shows the XRD patterns of samples SAM2, SAM3 and SAM4 samples, being all reflections indexed to the cubic perovskite structure of the $SrTiO_3$ phase (JCPDS file 35-0734) without any spurious phase.

The influence of MAH time on the crystallize size and the lattice parameter are presented in Table 1. It can be observed a reduction of both structural parameters with MAH treatment time. The behavior can be attributed to the larger amount of energy provided during the MAH treatment, which corroborates to reduce the defects in the $SrTiO_3$ network. Note that, the literature reports an $a_0$ value of approximately 3.905 Å.[23,37]

**Table 1** Average XRD crystallite size and lattice parameter ($a_0$) estimated from XRD patterns of the samples treated at 140 °C.

| Sample | MAH time (min) | Average crystallite size (nm) | $a_0$ (Å) | $\chi^2$ | $R_{wp}$ (%) |
|---|---|---|---|---|---|
| SAM2 | 10 | 74(1) | 3.9203(1) | 4.52 | 11.96 |
| SAM3 | 320 | 49(1) | 3.9181(1) | 4.52 | 7.04 |
| SAM4 | 640 | 45(1) | 3.9182(1) | 5.91 | 7.85 |

*$\chi^2$: is the square of goodness-of-fit indicator; $R_{wp}$: considered profile*

Fig. 3 shows the Ti K-edge XANES spectra of the samples SAM1, SAM2, SAM3 and SAM4 and the spectrum of the crystalline $SrTiO_3$ (used as a reference compound) prepared via polymeric precursor method, here designated as c-$SrTiO_3$.[38,42] The spectra revealed four pre-edge transitions, labeled as P1, P2, P3 and P4, as seen in the inset of Fig. 3. The physical origin of these electronic transitions is described elsewhere.[24,36,42]

First, it can be seen that the spectra of the samples synthesized via MAH route (SAM2, SAM3 and SAM4) are quite similar to the c-$SrTiO_3$ spectrum, which in turn is different from the SAM1 spectrum. Such results confirm that samples obtained via MAH route have a structure similar to the c-$SrTiO_3$ reference at short-and medium-range order around Ti atoms.

Regarding the influence of MAH synthesis time, the analysis of the pre-edge region shows that the intensity of peak P2 is higher for samples obtained via MAH method (SAM2, SAM3 and SAM4) than for c-$SrTiO_3$. Our research group has extensively investigated the local structure of $ATiO_3$ (A= Sr, Ba, Pb, or Ca) compounds using XAS spectroscopy.[8,23,24,27,31,36,42] These investigations reveal that the intensity of peak P2 is directly related to local symmetry of Ti cations.[24,31,42,47] Indeed, such electronic transition is related to $e_g$ orbitals, linked to Ti-O bonding, being sensitive to symmetry variations in the Ti environment.[23,24,48–51] Thus, the pre-edge region spectrum of c-$SrTiO_3$ (inset of Fig.3) is typical of titanates, where it is possible to find Ti cations coordinated by six oxygen anions, i.e., formed by $TiO_6$ clusters.[23,24,31] In contrast, it can be noticed that peak P2 is more intense in SAM2, SAM3 and SAM4 than in c-$SrTiO_3$, suggesting the existence of a mixture of $TiO_5$/$TiO_6$ clusters in samples obtained via MAH route, as illustrated in Fig.3.

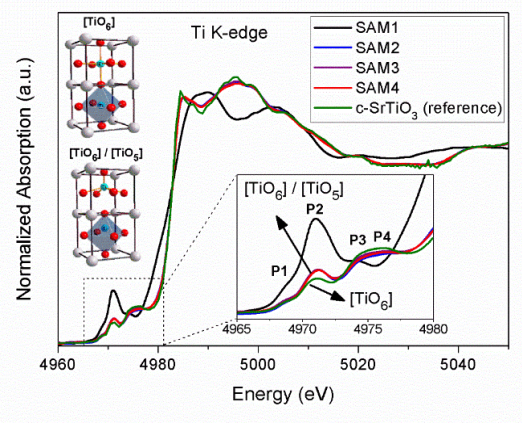


**Fig.3** Ti-K edge XANES spectra of samples SAM1, SAM2, SAM3 and SAM4 and the c-$SrTiO_3$ reference. The inset shows the pre-edge XANES region, illustrating the presence of $TiO_5$ and $TiO_6$ clusters.

It is important to note that although XRD results have confirmed a perfect long-range order for $SrTiO_3$ samples prepared via MAH route, the XANES spectra indicate a local disorder structure in the environment around Ti cations, which is not affected by synthesis time. The MAH system allows high reaction rates that favored here a fast crystallization of the $SrTiO_3$ phase. Despite exhibiting high order at long-range, this structure also presents a disorder in the local environment around Ti atoms.

The morphology of the as-obtained samples was studied via FE-SEM images. Fig. 4(a,b) show that SAM1 (without MAH treatment) consists of a non-homogeneous agglomeration of particles. These results are expected, since this sample contains different crystalline structures observed by XRD and XANES analyses. Fig. 4(c-f) reveal the formation of cube-like superstructures (or mesocrystals) as a consequence of the assembly of smaller cubes induced by MAH treatment.[24] In this way, even in a longer MAH time, such as 320 min, the as-observed morphology remains similar. Nevertheless, for samples treated during 640 min (SAM4), the cubes became more homogeneous and well-defined exhibiting a less quantity of assembled smaller cubes, as evidenced in Fig. 4(g-h).

It is known that the synthesis method plays an important role in order to obtain $SrTiO_3$ micro/nanostructures with different morphologies.[27,52] Our research group reported that the mediation of this process occurs due to the presence of OH groups adsorbed on the nanocrystals, leading to the formation of a specific configuration in which such crystals organize themselves into desired patterns through an oriented attachment (OA) mechanism, which could produce a defective single crystal with a spherical or cubic shape.[23] The presence of OH species on the samples surface was revealed by FTIR spectra, as displayed in Fig.S3 (ESI†). Thus, these small aggregates nanocrystals originated from the OA mechanism are responsible for increasing the crystal size when the coalescence occurs. [23,24,27,39,53,54]

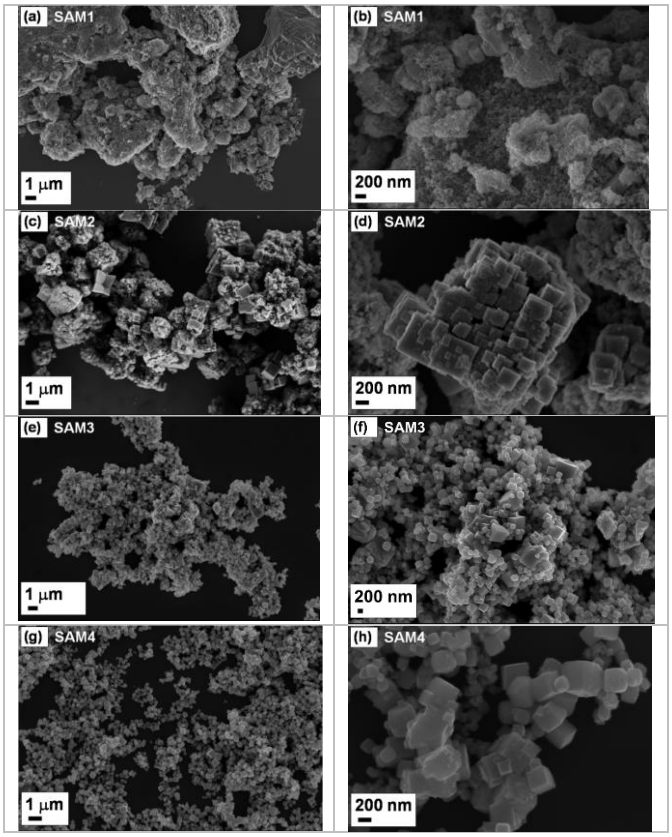


**Fig.4** FE-SEM images of samples (a,b) SAM1, (c,d) SAM2, (e,f) SAM3, and (g,h) SAM4.

Fig.5(a) shows the XPS survey spectra of the representative samples SAM2 and SAM4 and the c-$SrTiO_3$ reference. The peaks in these spectra were indexed, revealing the presence of the elements Sr, Ti, O and C. Beyond the peaks previously observed on the SAM4 XPS spectrum, it is also possible to identify a small peak assigned to K, a remainder of the mineralizing source.

In the high-resolution Sr 3d XPS spectra shown in Fig. 5(b), it is possible to observe two strong peaks located at 132.6 eV and 134.3 eV, which correspond to Sr(II) species on the surface of the samples.[55–57] The deconvolution of the Ti 2p XPS spectra, Fig. 5(c), reveals two main peaks at 458.3 and 464.0 eV attributed to Ti 2p3/2 and Ti 2p1/2 doublet core levels,[55,56,58] whose binding energy values were assigned to Ti(IV) species in $SrTiO_3$.[55–60] The correspondent O 1s spectra of SAM2, SAM4 and c-$SrTiO_3$ reference were deconvoluted into two components, as illustrated in Fig. 5(d). The standard deviation value of peak area was of ca. ±1.5%. The spectra exhibited similar characteristics, with the peak at around 529 eV corresponding to the oxygen lattice at the $SrTiO_3$ network.[55,56,58,61] The second component located at approximately 531 eV is attributed to $O^{2-}$ anions in the oxygen defect of the $SrTiO_3$ surface.[60] Tan and co-workers investigated the surface properties of $SrTiO_3$ nanocrystals applied as photocatalysts.[60] Based on XPS and electron paramagnetic resonance measurements, the authors observed a relationship between XPS peak area (at ca. 531 eV) and the concentration of oxygen vacancies on the $SrTiO_3$ surface.[60] As seen in Fig. 5(d), the peak area of the samples obtained via MAH route is larger than that of the reference sample (c-$SrTiO_3$), indicating the presence of a higher concentration of oxygen vacancies, especially on the crystal

surface. Furthermore, it can be observed that the increase in the MAH time favored the reduction of XPS peak area, suggesting the reduction of the oxygen vacancies on the sample surface.

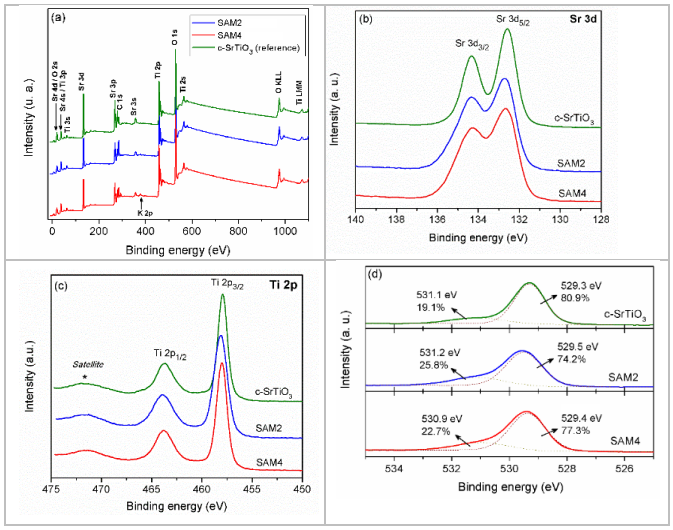


**Fig.5** XPS spectra of samples SAM2 and SAM4 and c-$SrTiO_3$. (a) Survey scan, (b) Sr 3d, (c) Ti 2p, and (d) O 1s core level spectra.

Fig. 6 shows the PL emission spectra of the samples SAM2, SAM3 and SAM4 and the c-$SrTiO_3$ reference. All the spectra exhibit a broad-band emission centered at ca. 470 nm (2.64 eV). The broad blue emission band is typical of compounds exhibiting intermediate electronic levels within the band gap where the relaxation process occurs along several paths, either involving additional levels located at the top of the O 2*p* valence band and lower conduction band 3*d* orbitals of Ti.[23,31,38,62–65] Fig.6 reveals a decrease of the PL intensity with MAH time, reaching a similar shape (intensity and profile) to the c-$SrTiO_3$ spectrum. As suggested by XPS results related to O vacancies, this behavior confirms that longer MAH times favor a reduction in the concentration of intrinsic defects created during the rapid crystallization process of $SrTiO_3$ phase via MAH method, probably oxygen vacancies. All these features show that the structural quality can be improved by increasing the reaction time, attaining the purpose of this work.

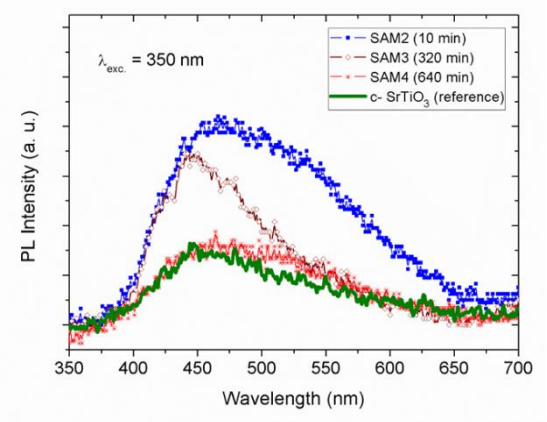


**Fig.6** PL spectra of samples SAM2, SAM3 and SAM4 at room temperature. For comparison purposes, the PL spectrum of the reference sample (c-$SrTiO_3$) was inserted.

The presence of oxygen vacancies, previously mentioned, was confirmed by using the electron paramagnetic resonance (EPR) technique. The EPR signal can be assigned to the paramagnetic oxygen vacancies,[60,66] which allow the formation of intermediary energy levels in the $SrTiO_3$ band gap, and consequently leading to broad PL emission presented in Fig.6.

Fig. 7 shows the electron paramagnetic resonance (EPR) spectra of samples SAM2, SAM3 and SAM4. The spectra present two EPR signals, the first one located at ca. 3381.5 G, corresponding to EPR $g_1$ = 1.932 signal, while the second one is located at 3421.6 G, corresponding to EPR $g_2$ = 1.910 signal. Regarding their amplitudes, the EPR $g_1$ signal presented values of approximately 0.1458, 0.2195 and 0.2435 for SAM2, SAM3, and SAM4, respectively. On the other hand, EPR $g_2$ signal values were of ca. 0.1870, 0.3057, and 0.1429 for SAM2, SAM3, and SAM4. Note that the behaviour of each center as a function of MAH time is quite different: intensity for $g_1$ enhances with MAH time, and that of $g_2$ exhibited a maximum for SAM3 sample. Based on these findings, it can be attributed that the competition of such centers (relative concentration) led to the reduction of PL emission intensity in the visible region (Fig. 6), and the maximum signal of $g_2$ can be assigned to the PL emission peak at ca. 440 nm for SAM3. In fact, the $g_1$ signal can be assigned to the peak at approximately 440 nm, and the $g_2$ to another one at approximately 510 nm. The sum of both emission bands, lead us to observe a maximum around 470 nm for SAM2 sample.

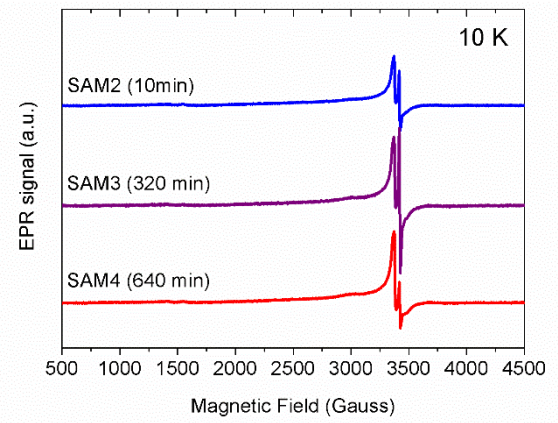


**Fig.7** Electron paramagnetic resonance (EPR) spectra of samples SAM2, SAM3 and SAM4.

## Conclusions

The main conclusions of the present work can be summarized as follows. i) The results point out the capability of the MAH method in preparing pristine $SrTiO_3$ powders in a short time and at a relatively lower temperature. ii) The combination of thermal and non-thermal effects present during MAH treatment provides ideal conditions for obtaining pristine $SrTiO_3$ phase. iii) The MAH method is not simply used to reduce the reaction time and temperature but also to suppress side reactions, improving the reproducibility. The results obtained by XRD, XANES and XPS techniques confirmed that this treatment is effective in eliminating spurious phases, unlike conventional annealing performed in electric oven. iv) FE-SEM

images reveal that the crystal growth process along the MAH route occurs via an assembly process, forming crystalline $SrTiO_3$ powders with cube-like morphologies. XPS results and PL emissions indicate that the increase in the treatment time contributes to a decrease in the defects found in the $SrTiO_3$ structure with concomitant enhancement of crystallization in the MAH route. vi) Finally, the present results go beyond the specific $SrTiO_3$ compound and can be extended to many ternary and more complex perovskite based oxides.

## Conflicts of interest

The authors declare no competing financial interest. There are no conflicts to declare.

## Acknowledgements

We thank Mr. Rorivaldo Camargo for operating the FE-SEM microscope and Prof. Otaciro R. Nascimento (IFSC/USP) by the EPR measurements. This research was partially performed at the Brazilian Laboratory of Synchrotron Radiation (LNLS; Project XAFS-20180311) and the Brazilian Nanotechnology National Laboratory (LNNano; Project XPS-22956), both in Campinas, SP, Brazil. The authors are also grateful for the financial support from the Brazilian research funding institutions CAPES (finance code 88887.197794/2018-00 and 001), CNPq (grant nos. 442076/2014-2, 311463/2017-7 and 405140/2018-5), FAPEG and FAPESP (grant nos. 2013/07296-2; 2017/12437-5). Prof. Juan Andrés acknowledges the financial support of the Universitat Jaume I (project UJIB2016-25), the Generalitat Valenciana (project PrometeoII/2014/022, ACOMP/2014/270, and ACOMP/2015/1202), and the Ministerio de Economia y Competitividad, Spain, (Project CTQ2015-65207-P).

## Notes and references

‡All authors have given the approval to the final version of the manuscript.

1 A. S. Bhalla, R. Guo and R. Roy, The perovskite structure – a review of its role in ceramic science and technology, *Mater. Res. Innov.*, 2000, **4**, 3–26.

2 S. Komarneni, R. Roy and Q. H. Li, Microwave-hydrothermal synthesis of ceramic powders, *Mater. Res. Bull.*, 1992, **27**, 1393–1405.

3 H. Y. Hwang, Perovskites: Oxygen vacancies shine blue, *Nat. Mater.*, 2005, **4**, 803–804.

4 H.-J. Kim and J.-H. Lee, Highly sensitive and selective gas sensors using p-type oxide semiconductors: Overview, *Sens. Actuators B Chem.*, 2014, **192**, 607–627.

5 G. Zhang, G. Liu, L. Wang and J. T. S. Irvine, Inorganic perovskite photocatalysts for solar energy utilization, *Chem. Soc. Rev.*, 2016, **45**, 5951–5984.

6 L. F. da Silva, A. C. Catto, W. Avansi Jr., L. S. Cavalcante, V. R. Mastelaro, J. Andrés, K. Aguir and E. Longo, Acetone gas sensor based on α-$Ag_2WO_4$ nanorods obtained via a microwave-assisted hydrothermal route, *J. Alloys Compd.*, 2016, **683**, 186–190.

7 L. F. da Silva, A. C. Catto, W. Avansi Jr, L. S. Cavalcante, J. Andres, K. Aguir, V. R. Mastelaro and E. Longo, A novel ozone gas sensor based on one-dimensional (1D) α-$Ag_2WO_4$ nanostructures, *Nanoscale*, 2014, **6**, 4058–4062.

8 A. C. Catto, L. F. da Silva, M. I. B. Bernardi, S. Bernardini, K. Aguir, E. Longo and V. R. Mastelaro, Local Structure and Surface Properties of $Co_xZn_{1-x}O$ Thin Films for Ozone Gas Sensing, *ACS Appl. Mater. Interfaces*, 2016, **8**, 26066–26072.

9 L. F. da Silva, W. Avansi Jr, A. C. Catto, J. E. F. S. Rodrigues, M. I. B. Bernardi and V. R. Mastelaro, The Role of Nb Addition in $TiO_2$ Nanoparticles: Phase Transition and Photocatalytic Properties, *Phys. Status Solidi A*, 2018, **125**, 1800321.

10 D. Segal, Chemical synthesis of ceramic materials, 1997, **7**, 1297–1305.

11 D. M. G. Leite, L. F. da Silva, A. L. J. Pereira and J. H. Dias da Silva, Nanocrystalline $Ga_{1-x}Mn_xN$ films grown by reactive sputtering, *J. Cryst. Growth*, 2006, **294**, 309–314.

12 Y.-T. Tseng, J.-C. Lin, Y.-J. Ciou and Y.-R. Hwang, Fabrication of a Novel Microsensor Consisting of Electrodeposited ZnO Nanorod-Coated Crossed Cu Micropillars and the Effects of Nanorod Coating Morphology on the Gas Sensing, *ACS Appl. Mater. Interfaces*, 2014, **6**, 11424–11438.

13 M. Baghbanzadeh, L. Carbone, P. D. Cozzoli and C. O. Kappe, Microwave-Assisted Synthesis of Colloidal Inorganic Nanocrystals, *Angew. Chemie Int. Ed.*, 2011, **50**, 11312–11359.

14 I. Bilecka and M. Niederberger, Microwave chemistry for inorganic nanomaterials synthesis, *Nanoscale*, 2010, **2**, 1358–1374.

15 A. Goktaş, A. Tumbul and F. Aslan, Grain size-induced structural, magnetic and magnetoresistance properties of $Nd_{0.67}Ca_{0.33}MnO_3$ nanocrystalline thin films, *J. Sol-Gel Sci. Technol.*, 2016, **78**, 262–269.

16 Y.-H. Huang, Z.-G. Xu, C.-H. Yan, Z.-M. Wang, T. Zhu, C.-S. Liao, S. Gao and G.-X. Xu, Soft chemical synthesis and transport properties of $La_{0.7}Sr_{0.3}MnO_3$ granular perovskites, *Solid State Commun.*, 2000, **114**, 43–47.

17 A. Goktas, A. Tumbul and F. Aslan, A new approach to growth of chemically depositable different ZnS nanostructures, *J. Sol-Gel Sci. Technol.*, 2019, **90**, 487–497.

18 K. J. Rao, B. Vaidhyanathan, M. Ganguli and P. a. Ramakrishnan, Synthesis of Inorganic Solids Using Microwaves, *Chem. Mater.*, 1999, **11**, 882–895.

19 A. de la Hoz, A. Diaz-Ortiz and A. Moreno, Microwaves in organic synthesis. Thermal and non-thermal microwave effects, *Chem. Soc. Rev.*, 2005, **34**, 164–178.

20 W. Shi, S. Song and H. Zhang, Hydrothermal synthetic strategies of inorganic semiconducting nanostructures, 2013, **42**, 5714–5743.

21 Y.-J. Zhu and F. Chen, Microwave-Assisted Preparation of Inorganic Nanostructures in Liquid Phase, *Chem. Rev.*, 2014, **114**, 6462–6555.

 

22 A. L. J. Pereira, L. Gracia, A. Beltrán, P. N. Lisboa-Filho, J. H. D. da Silva and J. Andrés, Structural and Electronic Effects of Incorporating Mn in $TiO_2$ Films Grown by Sputtering: Anatase versus Rutile, *J. Phys. Chem. C*, 2012, **116**, 8753–8762.

23 M. L. Moreira, V. M. Longo, W. Avansi, M. M. Ferrer, J. Andrés, V. R. Mastelaro, J. A. Varela and É. Longo, Quantum Mechanics Insight into the Microwave Nucleation of $SrTiO_3$ Nanospheres, *J. Phys. Chem. C*, 2012, **116**, 24792–24808.

24 L. F. da Silva, W. Avansi Jr, J. Andrés, C. Ribeiro, M. L. Moreira, E. Longo and V. R. Mastelaro, Long-range and short-range structures of cube-like shape $SrTiO_3$ powders: microwave-assisted hydrothermal synthesis and photocatalytic activity., *Phys. Chem. Chem. Phys.*, 2013, **15**, 12386–93.

25 M. L. Moreira, G. P. Mambrini, D. P. Volanti, E. R. Leite, M. O. Orlandi, P. S. Pizani, V. R. Mastelaro, C. O. Paiva-Santos, E. Longo and J. A. Varela, Hydrothermal Microwave: A New Route to Obtain Photoluminescent Crystalline $BaTiO_3$ Nanoparticles, *Chem. Mater.*, 2008, **20**, 5381–5387.

26 J. Sun, W. Wang and Q. Yue, Review on Microwave-Matter Interaction Fundamentals and Efficient Microwave-Associated Heating Strategies, *Materials (Basel).*, 2016, **9**, 231.

27 L. F. da Silva, W. Avansi Jr, M. L. Moreira, A. Mesquita, L. J. Q. Maia, J. Andrés, E. Longo and V. R. Mastelaro, Relationship between Crystal Shape, Photoluminescence, and Local Structure in $SrTiO_3$ Synthesized by Microwave-Assisted Hydrothermal Method, *J. Nanomater.*, 2012, **2012**, 890397.

28 I. Bilecka, L. Luo, I. Djerdj, M. D. Rossell, M. Jagodic, Z. Jaglicic, Y. Masubuchi, S. Kikkawa and M. Niederberger, Microwave-Assisted Nonaqueous Sol–Gel Chemistry for Highly Concentrated ZnO-Based Magnetic Semiconductor Nanocrystals, *J. Phys. Chem. C*, 2011, **115**, 1484–1495.

29 G. A. Tompsett, W. C. Conner and K. S. Yngvesson, Microwave Synthesis of Nanoporous Materials, *ChemPhysChem*, 2006, **7**, 296–319.

30 M. Godinho, C. Ribeiro, E. Longo and E. R. Leite, Influence of Microwave Heating on the Growth of Gadolinium-Doped Cerium Oxide Nanorods, *Cryst. Growth Des.*, 2008, **8**, 384–386.

31 V. M. Longo, A. T. de Figueiredo, S. de Lazaro, M. F. Gurgel, M. G. S. Costa, C. O. Paiva-Santos, J. A. Varela, E. Longo, V. R. Mastelaro, F. S. DE Vicente, A. C. Hernandes and R. W. A. Franco, Structural conditions that leads to photoluminescence emission in $SrTiO_3$: An experimental and theoretical approach, *J. Appl. Phys.*, 2008, **104**, 23515.

32 J. Li, S. Li, F. Liu, M. A. Alim and G. Chen, The origin of varistor property of $SrTiO_3$-based ceramics, *J. Mater. Sci. Mater. Electron.*, 2003, **14**, 483–486.

33 O. K. Tan, W. Cao, Y. Hu and W. Zhu, Nano-structured oxide semiconductor materials for gas-sensing applications, *Ceram. Int.*, 2004, **30**, 1127–1133.

34 J. H. Haeni, P. Irvin, W. Chang, R. Uecker, P. Reiche, Y. L. Li, S. Choudhury, W. Tian, M. E. Hawley, B. Craigo, A. K. Tagantsev, X. Q. Pan, S. K. Streiffer, L. Q. Chen, S. W. Kirchoefer, J. Levy and D. G. Schlom, Room-temperature ferroelectricity in strained $SrTiO_3$, *Nature*, 2004, **430**, 758–761.

35 M. Moniruddin, K. Afroz, Y. Shabdan, B. Bizri and N. Nuraje, Hierarchically 3D assembled strontium titanate nanomaterials for water splitting application, *Appl. Surf. Sci.*, 2017, **419**, 886–892.

36 L. F. da Silva, O. F. Lopes, V. R. de Mendonça, K. T. G. Carvalho, E. Longo, C. Ribeiro and V. R. Mastelaro, An Understanding of the Photocatalytic Properties and Pollutant Degradation Mechanism of $SrTiO_3$ Nanoparticles, *Photochem. Photobiol.*, 2016, **92**, 371–378.

37 V. R. Calderone, A. Testino, M. T. Buscaglia, M. Bassoli, C. Bottino, M. Viviani, V. Buscaglia and P. Nanni, Size and Shape Control of $SrTiO_3$ Particles Grown by Epitaxial Self-Assembly, *Chem. Mater.*, 2006, **18**, 1627–1633.

38 L. F. da Silva, L. J. Q. Maia, M. I. B. Bernardi, J. A. Andrés and V. R. Mastelaro, An improved method for preparation of $SrTiO_3$ nanoparticles, *Mater. Chem. Phys.*, 2011, **125**, 168–173.

39 L. F. da Silva, W. Avansi, M. L. Moreira, J. Andres, E. Longo and V. R. Mastelaro, Novel $SrTi_{1-x}Fe_xO_3$ nanocubes synthesized by microwave-assisted hydrothermal method, *CrystEngComm*, 2012, **14**, 4068–4073.

40 L. F. da Silva, M. I. B. Bernardi, L. J. Q. Maia, G. J. M. Frigo and V. R. Mastelaro, Synthesis and thermal decomposition of $SrTi_{1-x}Fe_xO_3$ ($0.0 \leq x \leq 0.1$) powders obtained by the polymeric precursor method, *J. Therm. Anal. Calorim.*, 2009, **97**, 173–177.

41 L. F. da Silva, V. R. Mastelaro, A. C. Catto, C. A. Escanhoela Jr., S. Bernardini, S. C. Zílio, E. Longo and K. Aguir, Ozone and nitrogen dioxide gas sensor based on a nanostructured $SrTi_{0.85}Fe_{0.15}O_3$ thin film, *J. Alloys Compd.*, 2015, **638**, 374–379.

42 L. F. da Silva, J.-C. M'Peko, J. Andrés, A. Beltrán, L. Gracia, M. I. B. Bernardi, A. Mesquita, E. Antonelli, M. L. Moreira and V. R. Mastelaro, Insight into the Effects of Fe Addition on the Local Structure and Electronic Properties of $SrTiO_3$, *J. Phys. Chem. C*, 2014, **118**, 4930–4940.

43 M. Bender, E. Gagaoudakis, E. Douloufakis, E. Natsakou, N. Katsarakis, V. Cimalla, G. Kiriakidis, E. Fortunato, P. Nunes, A. Marques and R. Martins, Production and characterization of zinc oxide thin films for room temperature ozone sensing, *Thin Solid Films*, 2002, **418**, 45–50.

44 M. L. Moreira, E. C. Paris, G. S. do Nascimento, V. M. Longo, J. R. Sambrano, V. R. Mastelaro, M. I. B. Bernardi, J. Andrés, J. A. Varela and E. Longo, Structural and optical properties of $CaTiO_3$ perovskite-based materials obtained by microwave-assisted hydrothermal synthesis: An experimental and theoretical insight, *Acta Mater.*, 2009, **57**, 5174–5185.

45 A. Michalowicz, J. Moscovici, D. Muller-BouvetDiane and K. Provost, MAX: Multiplatform Applications for XAFS, *J. Phys. Conf. Ser.*, 2009, **190**, 12034.

46 S. Aydogan, M. Erdemoğlu, A. Aras, G. Uçar and A. Özkan, Dissolution kinetics of celestite ($SrSO_4$) in HCl solution with BaCl2, *Hydrometallurgy*, 2006, **84**, 239–246.

47 A. C. Catto, L. F. da Silva, C. Ribeiro, S. Bernardini, K. Aguir, E. Longo and V. R. Mastelaro, An easy method of preparing ozone gas sensors based on ZnO nanorods, *RSC Adv.*, 2015, **5**, 19528–19533.

48 A. M. Ruiz, G. Dezanneau, J. Arbiol, A. Cornet and J. R. Morante, Insights into the Structural and Chemical Modifications of Nb

Additive on $TiO_2$ Nanoparticles, *Chem. Mater.*, 2004, **16**, 862–871.

49 R. V. Vedrinskii, V. L. Kraizman, A. A. Novakovich, Ph. V. Demekhin and S. V. Urazhdin, Pre-edge fine structure of the 3d atom K x-ray absorption spectra and quantitative atomic structure determinations for ferroelectric perovskite structure crystals, *J. Phys. Condens. Matter*, 1998, **10**, 9561.

50 D. Barreca, D. Bekermann, E. Comini, A. Devi, R. A. Fischer, A. Gasparotto, C. Maccato, C. Sada, G. Sberveglieri and E. Tondello, Urchin-like ZnO nanorod arrays for gas sensing applications, *CrystEngComm*, 2010, **12**, 3419–3421.

51 V. Krayzman, I. Levin, J. C. Woicik, D. Yoder and D. A. Fischer, Effects of local atomic order on the pre-edge structure in the Ti K X-ray absorption spectra of perovskite $CaTi_{1-x}Zr_xO_3$, *Phys. Rev. B*, 2006, **74**, 224104.

52 M. Ye, M. Wang, D. Zheng, N. Zhang, C. Lin and Z. Lin, Garden-like perovskite superstructures with enhanced photocatalytic activity, *Nanoscale*, 2014, **6**, 3576–3584.

53 G. Canu and V. Buscaglia, Hydrothermal synthesis of strontium titanate: thermodynamic considerations, morphology control and crystallisation mechanisms, *CrystEngComm*, 2017, **19**, 3867–3891.

54 W. Avansi Jr, L. J. Q. Maia, C. Ribeiro, E. R. Leite and V. R. Mastelaro, Local structure study of vanadium pentoxide 1D-nanostructures, *J. Nanoparticle Res.*, 2011, **13**, 4937.

55 S. Zhang, D. Guo, M. Wang, M. S. Javed and C. Hu, Magnetism in $SrTiO_3$ before and after UV irradiation, *Appl. Surf. Sci.*, 2015, **335**, 115–120.

56 L. Gu, H. Wei, Z. Peng and H. Wu, Defects enhanced photocatalytic performances in $SrTiO_3$ using laser-melting treatment, *J. Mater. Res.*, 2017, **32**, 748–756.

57 O. Lobacheva, Y. M. Yiu, N. Chen, T. K. Sham and L. V Goncharova, Changes in local surface structure and Sr depletion in Fe-implanted $SrTiO_3$ (001), *Appl. Surf. Sci.*, 2017, **393**, 74–81.

58 R. P. Vasquez, $SrTiO_3$ by XPS, *Surf. Sci. Spectra*, 1992, **1**, 129–135.

59 V. V Atuchin, V. G. Kesler, N. V Pervukhina and Z. Zhang, Ti 2p and O 1s core levels and chemical bonding in titanium-bearing oxides, *J. Electron Spectros. Relat. Phenomena*, 2006, **152**, 18–24.

60 H. Tan, Z. Zhao, W. Zhu, E. N. Coker, B. Li, M. Zheng, W. Yu, H. Fan and Z. Sun, Oxygen Vacancy Enhanced Photocatalytic Activity of Pervoskite $SrTiO_3$, *ACS Appl. Mater. Interfaces*, 2014, **6**, 19184–19190.

61 J.-C. Dupin, D. Gonbeau, P. Vinatier and A. Levasseur, Systematic XPS studies of metal oxides, hydroxides and peroxides, *Phys. Chem. Chem. Phys.*, 2000, **2**, 1319–1324.

62 A. E. Souza, G. T. A. Santos, B. C. Barra, W. D. Macedo, S. R. Teixeira, C. M. Santos, A. M. O. R. Senos, L. Amaral and E. Longo, Photoluminescence of $SrTiO_3$: Influence of Particle Size and Morphology, *Cryst. Growth Des.*, 2012, **12**, 5671–5679.

63 W. F. Z. and Z. Y. and M. S. Z. and Z. L. D. and W. C. Chen, Roles of defects and grain sizes in photoluminescence of nanocrystalline $SrTiO_3$, *J. Phys. Condens. Matter*, 1999, **11**, 5655.

64 A. Rubano, D. Paparo, F. M. Granozio, U. Scotti di Uccio and L. Marrucci, Blue luminescence of $SrTiO_3$ under intense optical excitation, *J. Appl. Phys.*, 2009, **106**, 103515.

65 G. Blasse, On the luminescence of $SrTiO_3$ and related titanates, *Mater. Res. Bull.*, 1983, **18**, 525–528.

66 H. Trabelsi, M. Bejar, M. P. F. Graça, M. A. Valente, M. J. Soares and N. A. Sobolevi, Raman, EPR and ethanol sensing properties of oxygen-vacancies $SrTiO_{3-\delta}$ compounds, *Appl. Surf. Sci.*, 2017, **426**, 386–390.